

**Wind Stress Forcing of the North Sea "Pole Tide"**

*IN-41  
0408 2005*

**William P. O'Connor**  
NOAA/NOS Coast Survey Development Laboratory, N/CS13  
1315 East-West Highway, Silver Spring, MD 20910-3282, USA

**Benjamin Fong Chao**  
Space Geodesy Branch, Code 926  
NASA Goddard Space Flight Center, Greenbelt, MD 20771, USA

**Dawei Zheng**  
Shanghai Astronomical Observatory, Chinese Academy of Sciences, Shanghai 200030, China

**Andrew Y. Au**  
Raytheon ITSS, Lanham, MD 20706, USA

key words: North Sea, sea level, tides, winds, Chandler wobble

(corresponding author: Benjamin F. Chao)

*to be submitted to Geophys. J. Int.*



## **SUMMARY**

We conducted numerical simulations of the wind-forcing of the sea level variations in the North Sea using a barotropic ocean model with realistic geography, bathymetry, and boundary conditions, to examine the forcing of the 14-month “pole tide” which is known to be strong along the Denmark-Netherlands coast. The simulation input is the monthly-mean surface wind stress field from the National Centers for Environmental Prediction (NCEP) reanalysis for the 40-year period 1958-1997. The output sea level response was then compared with 10 coastal tide gauge records from the Permanent Service for Mean Sea Level (PSMSL). Besides the strong seasonal variations, several prominent quasi-periodicities exist at around 7 years, 3 years, 14 months, 9 months, and 6.5 months. Correlation and spectral analyses show remarkable agreement between the model output and the observations, particularly in the 14-month, or Chandler period band. The latter indicates that the enhanced pole tide found in the North Sea along the Denmark-Netherlands coast is actually the coastal setup response to wind stress forcing with a periodicity of 14 months. We find no need to invoke a geophysical explanation involving resonance-enhancement of pole tide in the North Sea to explain the observations.

## **1. INTRODUCTION**

In this paper we reconsider the following question: Is the anomalously large 14-month “pole tide” observed at the tide gauge stations along the continental coast of the North Sea really the pole tide that is somehow enhanced, or is it primarily of direct meteorological origin (and hence not really the “pole tide”) forced by the regional surface wind stress with a 14-month periodicity? Our results strongly support the latter.

The polar motion of the earth's rotational axis sets up the pole tide in the ocean via the centrifugal potential induced by the polar motion. In particular, the 14-month Chandler wobble in the polar motion generates a 14-month pole tide. At this long period, there is little horizontal motion associated with the pole tide and the height is close to the equilibrium value, or height the tide would have if all the wobble potential energy were used to raise the sea level. Theoretical studies by Dickman (1985, 1988) and others have shown that the pole tide in the deep oceans should be near its equilibrium value. The maximum amplitude of an equilibrium pole tide is about 0.5 cm at 45° latitude. Independent data studies over the past several decades (for a review, see, e.g., Lambeck 1980, p.

212-214) have shown that while the pole tide amplitude is generally near the equilibrium tide value, it is anomalously large, up to 3 cm, in parts of the North and Baltic Seas. A salient feature in the North Sea is the enhanced 14-month tide along the continental coast known as the eastward intensification (e.g., Xie & Dickman 1995), where the tidal amplitude increases sharply eastward along the Denmark-Netherlands coast to five times its equilibrium value (Miller & Wunsch 1973, Fig. 2, reproduced in Lambeck, 1980, Fig. 8.1). A number of studies, most recently by Ekman & Stigebrandt (1990), have concluded that the secular change in the pole tide, especially in the North and Baltic Seas, is not correlated with the pole tide forcing, and have suggested a meteorological component to the forcing.

Analytical and numerical studies of the dynamics of the pole tide in the North Sea have been made by Wunsch (1974, 1986), Dickman & Preisig (1986), Carton & Wahr (1986), and Xie & Dickman (1995). These are mentioned by Wunsch *et al.* (1997) who discuss the possibility of a basin resonance in the North Sea at the pole tide period. No satisfactory explanation has yet been given for the enhancement of the North Sea pole tide along the continental coast as a result of the direct pole tide forcing, the forcing by the global tide as an open boundary condition, or any possible resonance phenomenon with a 14-month period. These possibilities were considered and rejected years ago by Miller (1973), who then suggested that the wind stress was the most probable cause of the observed 14-month tide. Indeed, these studies collectively show that a pole tide enhancement cannot be derived from any homogeneous system of equations describing the flow regime in the North Sea. An analytic study by O'Connor (1986) showed that the eastward intensification can be explained in terms of an inhomogeneous (forced) system of equations with a linear dynamical model for an idealized rectangular basin, assuming that the forcing is a small change in the east-west wind stress component near the 14-month Chandler period.

The North Sea climate is strongly influenced by the changes in the North Atlantic wind field (WASA Group 1998). There is evidence for a periodic 14-month oscillation in sea surface pressure over the North Atlantic, North Sea, and Baltic Sea regions, which is directly related to an oscillation in the position of the Icelandic low as part of the North Atlantic Oscillation system (e.g., Wallace & Gutzler 1981). This was demonstrated by Bryson & Starr (1977) who analyzed a National Center for Atmospheric Research (NCAR) global monthly mean sea level pressure data set for the period 1900-1970. Other previous investigations into this phenomenon are listed by O'Connor (1986) and Tsimplis, Flather & Vassie (1994). Two observational studies investigated periodicities in the

14-month meteorological forcing over the North Sea region and their correlation with the pole tide observations there. The first study was by Trupin & Wahr (1990) who used the NCAR monthly mean sea surface pressure data. They concluded that the pole tide in the North Sea was correlated with the atmospheric pressure at that 14-month period. It might have been more appropriate to make a correlation with the north-south pressure gradient in that region, since this determines the east-west component of the wind through the geostrophic relation, modified by friction in the boundary layer. In the second study, Tsimplis *et al.* (1994) used a 30-year time series of wind and pressure data from the Norwegian Meteorological Institute and tidal specifications on the northern open boundary to run a numerical tide and surge model of the North Sea. They concluded that the pole tide along the continental coast was the result of a variation in the east-west wind stress with a 14-month periodicity. However, there remains some controversy on whether the amplitude and phase of the wind forcing spectral peak over the North Sea is sufficient to account for the sea level response near the Chandler period. This is reflected in the comments of Wunsch *et al.* (1997) on the work of Tsimplis *et al.* (1994).

We shall re-investigate this problem with a new, and hopefully more complete meteorological data set and a North Sea ocean model. Historically, meteorological data sets have been compiled only from observations. More recently, output of global numerical weather prediction models assimilating all available observational data are being used to make climatologies. The data for the surface winds are accepted as generally accurate because they are representative of the large scale flow. We shall adopt the 40-year reanalysis product of the National Centers for Environmental Prediction (NCEP) (Kalnay *et al.* 1996). Figure 1 depicts the geography of the region studied, as well as its average NCEP surface wind stress field (see below), which we use to force a barotropic North Sea ocean model generally following the approach of Tsimplis *et al.* (1994). We compare our model output, or “computed” sea level with actual observations for 10 continental coastal stations from the Permanent Service for Mean Sea Level (PSMSL). Good agreement is found, including in the Chandler frequency band, indicating that the enhanced “pole tide” in the North Sea is specifically the coastal setup response to wind stress forcing with a periodicity of 14 months.

## **2. OBSERVED SEA LEVELS**

The PSMSL (URL <http://www.nbi.ac.uk/psmsl/psmsl.info.html>) archives monthly sea level records

from tide gauge stations worldwide. For the North Sea, it provides 17 station records that started prior to 1958 (and many more records that are shorter). Thirteen of them are on the continental coast, and we examine 10 of these stations (Fig. 1) from the English Channel to Denmark, where the pole tide amplitude becomes pronounced. They are, from north to south: Esbjerg, West-Terschelling, Delfzijl, Harlingen, Den Helder, IJmuiden, Hoek Van Holland, Maassluis, Vlissingen, Oostende (see Table 1). The northern stations are known to have the strongest 14-month tide showing the eastward intensification; the first five stations are thus combined later for the purpose of studying this signal.

### 3. COMPUTED SEA LEVELS

#### 3.1 Atmospheric wind stress forcing

A description of the monthly mean wind directions and persistency at various locations over the North Sea is given by Korevaar (1990). During the period 1961-1980 the prevailing annual wind direction was from the SW to WNW. The seasonal variation was such that in summer the wind was from WNW to NW, while in winter it was from SW to W. In the spring and fall, the winds can be from several directions, and the monthly wind direction can have an easterly component. Also, the strongest winds usually have a westerly component. This information is well known, but here we want to make use of the latest meteorological data to search for interested periodicities in the wind forcing of the North Sea.

The global data set of the NCEP reanalysis (Kalnay *et al.* 1996) for the 40-year period Jan. 1958 - Dec. 1997 contains monthly mean data for a large number of variables. We first examine directly the low level 1000 millibar (mb) winds in the air-sea boundary layer. The NCEP data set has the monthly mean values for the eastward (u) and northward (v) horizontal components, given at  $2.5^\circ \times 2.5^\circ$  intervals. Those points over the North Sea and immediately surrounding region that are used in this study are at the intersection of longitudes  $5.0^\circ$  W,  $2.5^\circ$  W,  $0^\circ$ ,  $2.5^\circ$  E,  $5.0^\circ$  E,  $7.5^\circ$  E,  $10.0^\circ$  E, and latitudes  $50.0^\circ$  N,  $52.5^\circ$  N,  $55.0^\circ$  N,  $57.5^\circ$  N,  $60.0^\circ$  N.

Figure 2 summarizes the behavior of the NCEP u and v wind fields of the North Sea region, averaged over the above grid points. Fig. 2(b) gives their maximum-entropy power spectra, where the order of the corresponding autoregressive model is selected according to criteria in Marple (1990), about 20% of the record length in our case. While not surprisingly both show strong annual

power, the  $u$  component has a rich ensemble of periodicities, including a prominent signal at the Chandler period near 14 months. The latter, as we show later, is the major driving source of the observed 14-month signal in the sea level. The  $v$  component did not exhibit strong periodicities other than the annual.

The parameter we use to directly force the ocean model is the horizontal wind stress vector on the sea surface,  $\tau = (\tau_x, \tau_y)$ , which is a quadratic function of the surface wind velocity  $\mathbf{V}=(u,v)$ :

$$\tau = \rho C_d \mathbf{V} |\mathbf{V}| \quad (1)$$

where  $\rho$  is the surface layer air density and  $C_d$  is the drag coefficient. The air density varies only slightly with air temperature and humidity. The drag coefficient is a function of both the wind speed and the atmospheric surface layer stability. The air-sea temperature difference and heat flux increase momentum transfer due to turbulence at the air-sea interface. These stability effects can cause the drag coefficient to significantly vary seasonally and spatially. The NCEP global model uses a surface layer parameterization to calculate the wind stress (e.g. Haltiner & Williams 1980, section 8-6). The drag coefficient is calculated by the formula  $C_d = k^2 / [\ln(z/z_0) - \psi(z/L)]^2$ , where  $k=0.4$  is the von Karman constant,  $z$  is the first model level (usually 30 - 40 m),  $z_0$  is the roughness length,  $L$  is the Monin-Obukhov length scale which depends on turbulent fluxes, and  $\psi$  is an empirical stability function. This latter depends on the Richardson number, which relates the turbulence production due to wind shear to the turbulence damping due to the stratification, resulting from air-sea temperature differences. In fact, the value of the 10 m wind velocity can be found from  $\mathbf{V} = (\mathbf{V}^*/k) [\ln(z/z_0) - \psi(z/L)]$ , where  $\mathbf{V}^*$  is the friction velocity, which can be related to the roughness length over water by the Charnock relation  $z_0 = 0.014 \mathbf{V}^{*2}/g$ , where  $g$  is the acceleration of gravity. The equations are solved numerically by iteration.

The NCEP wind stress data are given at intervals of 1.875° in longitude and 1.904° in latitude. The points over the North Sea and surrounding region that are used in this study are at the intersections of longitudes 3.75° W, 1.875° W, 0°, 1.875° E, 3.75° E, 5.625° E, 7.5° E, 9.375° E, and latitudes 48.571° N, 50.475° N, 52.38° N, 54.285° N, 56.189° N, 58.094° N, 59.99° N. Fig. 1 shows the “prevailing”, 40-year average of these monthly NCEP wind stress fields at these grid points. This compares favorably with the annual mean wind stress over the North Sea given by Hellerman (1967), who found some spatial variability in the annual wind stress pattern with the

representative values  $\tau_x = 0.062 \text{ nt m}^{-2}$ ,  $\tau_y = 0.021 \text{ nt m}^{-2}$ .

The NCEP wind stresses were calculated at 40-minute time step intervals, from which a daily average was made. The daily wind stress output of the NCEP model was then averaged to form the monthly mean values. Note that the monthly averaging must be invoked on the wind stress values after they are computed from the wind velocity, rather than on the wind velocity itself prior to calculation of wind stress. This is because the averaging of wind velocity would tend to reduce the resultant wind stress due to the quadratic nature of Eq. 1 (see below for more discussion).

We made an alternate wind stress calculation as a check on the NCEP surface wind stress output. This was for neutral stability conditions, where the air-sea temperature difference was neglected. This has been done in previous studies when the air-sea temperatures and stability conditions were unobtainable. The wind stress was calculated directly from equation (1) with the NCEP 1000 mb winds used in place of 10 m surface winds, a neutral drag coefficient, and the constant air density  $1.2 \text{ kg m}^{-3}$ . A climatology of the global ocean wind stress based on ECMWF 1000 mb winds was produced by Trenberth, Large & Olson (1989) for the years 1980-1986, during which only the 1000 mb winds were available. As explained by Trenberth *et al.* (1989), the ship wind observations were assigned to the 1000 mb level and effectively represent 10 m winds. However, an evaluation of ECMWF-based climatological wind stress fields by Mestas-Nunez *et al.* (1994) concluded that the 1000 mb winds were more representative of winds at a height of 30 m, and the resulting wind stresses of Trenberth *et al.* (1989) were too large by 50%.

The drag coefficient depends on the sea state (waves, swell) and is written as a linear function of wind speed. A representative value for the North Sea determined from, e.g., Smith *et al.* (1992) is  $C_N = (0.50 + 0.091 |V|) \times 10^{-3}$ , where the wind speed is in  $\text{ms}^{-1}$ . The wind stresses calculated under neutral conditions with the 1000 mb mean monthly winds were smaller than the wind stresses produced directly by the NCEP model by about a factor of five. This is explained by the fact that the wind stress is proportional to the square (or even cube) of the wind speed, and so the momentum input is strongly influenced by the high wind events. The monthly averaging done on the 1000 mb wind velocity itself smooths out these high wind events (see above), and this is at least partly why our neutral stability calculation significantly underpredicts the wind stress. Other researchers (e.g., Stammer *et al.* 1996) have noted that if an ocean model does not resolve eddies and have the correct heat flux surface conditions, it can underpredict the sea level and its variability by a factor of over 2.

In our present application, we conclude that the NCEP wind stress calculation should be more

accurate. It will be adopted for our ocean model forcing below.

### 3.2 North Sea dynamics and model

The flow in the North Sea has been studied using numerical models (see Sundermann & Lenz 1983 for a review). These models have had great success in modeling the sea level and currents in response to tidal and wind forcing. They include both realistic coastlines and bottom topography. Tides and wind forced surges in the North Sea can be modeled adequately with barotropic models, which solve for the sea level and the vertically averaged currents (Flather 1984; Verboom, de Ronde & van Dijk 1992). The numerical model used by Tsimplis *et al.* (1994) is described by Flather, Proctor & Wolf (1991). We will use the numerical ocean model developed at Princeton University and described by Blumberg & Mellor (1987), written in generalized coordinates. Since we desire to investigate the wind forced sea level set up along the continental coast, we can use the barotropic subset of these model equations. These are the flux form of the vertically integrated nonlinear continuity and horizontal momentum equations, which are solved for the sea level and the horizontal components of velocity. In spherical coordinates, the horizontal momentum equations consist of terms for the local time derivative and horizontal advective terms, the Coriolis acceleration, sea level pressure gradient, tangential wind stress on the sea surface, and quadratic bottom friction with a constant drag coefficient of 0.0025. The system of equations is solved using a finite differencing scheme that is centered in time and space on the Arakawa-C grid.

The model North Sea domain (Fig. 1) covers the region from 51° N to 59° N latitude, and from 3° W to 9° E longitude. There are 97 grid points in the north-south with a spacing of 5' in latitude (9.27 km), and 73 grid points in the east-west with a spacing of 10' in longitude (9.55 - 11.66 km). The bathymetry was digitized from the British Admiralty charts 2182A, 2182B, and 2182C. Over most of the North Sea the depths were taken at intervals of 15' latitude by 30' longitude and then interpolated to the finer grid with a bilinear interpolation scheme. However, in order to accurately model the wind forced setup along the European coast, the depths either south of 54° N latitude or east of 7° E longitude were digitized at intervals of 5' latitude and 10' longitude. The grid size did not permit resolution of the barrier islands and channels to ports along the continental coast. Thus comparisons with tide gage data at some ports were made with the water level data from the closest model grid points. The shallowest depths recorded were 3 m along the continental coast, while the

deepest was 570 m in the Norwegian Trench. Any grid point depths shallower than 100 m along the Norwegian coast were made land points. The domain was closed along the southern, western and eastern boundaries to avoid problems with unnecessary open boundaries. A time step of 60 s is short enough to ensure computational stability.

We now describe the dynamics of a residual circulation, which is the mean velocity field averaged over a period of at least several days, to cancel transitory wind currents and tidal oscillations. The flow in the North Sea can be influenced by the open boundary conditions, the atmospheric pressure gradient (inverted barometer effect), and the wind stress. The work of Timmerman (1977, p.47-49), Prandle (1975), and Flather (1984) indicates that the sea level and circulation in the southern North Sea are predominantly the result of the wind stress, rather than the atmospheric pressure gradient. Tsimplis *et al.* (1994) included the semi-diurnal and diurnal tidal forcing as open boundary conditions and showed that this had no effect on the 14-month tide. Carton & Wahr (1986) showed that using the deep ocean pole tide as an open boundary condition resulted in raising the elevation of the basin without a sea level gradient along the continental coast. Accordingly, only the wind stress forcing will be considered in this study.

When the winds are steady or slowly varying in time, the model is not sensitive to the open northern boundary conditions which is removed from the region of our main interest, the continental Denmark-Netherlands coast. The equations are linearized at the northern boundary, and a radiation condition is used there:  $v = (g/H)^{1/2} \eta - \tau_x / (\rho_o f H)$ , where  $H$  is the depth,  $\eta$  is the sea level,  $\rho_o$  is the seawater density, and  $f$  is the value of the Coriolis parameter at 59° N latitude. We have seen that the seasonal and 14-month periodic wind stresses over the North Sea have a strong eastward component. This boundary condition is particularly well suited for modeling the flow due to winds with a strong eastward component, since it allows for southward Ekman drift into the North Sea across most of the northern boundary, and northward geostrophic outflow near the eastern boundary, as discussed by O'Connor (1986).

### 3.3 Model tests

The North Sea model used is a one layer barotropic hydrodynamic model forced only by the wind stress and does not consider density changes. The amplitude of the ocean model sea level depends on the model parameters (the bathymetry and coastline, bottom friction coefficient, and open

boundary conditions at the northern boundary), in addition to the wind stress forcing. The model grid does not resolve the barrier islands and channels to ports along the continental coast. In some cases the tide gauges are at ports inside of barrier islands. Presumably, the amplitudes could be improved by engineering the drag coefficient, friction, and station depths until better agreement is reached, as is typically done for storm surge models. In the ocean the annual cycle in sea level is the result of both the wind stress forcing and the steric effects due to density changes from temperature and salinity variations.

Despite this limitation of the barotropic model, one way to tell how "good" it is can be seen by running the model with a constant annual average wind stress, and looking at the setup in sea level along the continental coast. As a first test, the North Sea model was run with this constant 40-year average NCEP wind stress forcing (Fig. 1). The average stress for NCEP grid points were interpolated to the ocean model grid with a bilinear interpolation scheme. The model was then run until a steady state resulted after three days. The resulting sea levels and currents are shown in Fig. 3, with an evident eastward intensification of sea level along the continental coast. In particular there is a maximum setup of about 12 cm along the Denmark coast. These results are in very close agreement with the results of Prandle (1978) and Davies (1982), who forced models of the North Sea with an average annual wind stress. These results are also in agreement with the observational studies of Pattullo *et al.* (1955) and Rossiter (1967), which show that the mean annual sea level and amplitude of the seasonal oscillation exhibit a steep gradient along the Netherlands coast, which they attributed to eastward winds and atmospheric pressure.

The residual circulation that results from these eastward winds is a counterclockwise gyre over the North Sea, as a consequence of the slope of the bottom topography. This has been shown by analytical models with north-south bottom slope (Furnes 1980, O'Connor 1986). However, realistic bathymetry is necessary to obtain the strong sea level gradients along the continental coast. In the deeper northern part, there is inflow due to Ekman transport. Water piles up in the shallow German Bight and flows northward along the continental coast in a geostrophic boundary current. This gives rise to a sea level gradient along the Netherlands coast. This is shown clearly in the numerical modeling studies of Maier-Reimer (1977), Prandle (1978; 1984), Pingree & Griffiths (1980), Davies (1982), and Backhaus & Maier-Reimer (1983). It should be noted that storm surge models of the North Sea show that when there are strong persistent westerly winds for a day or longer, there is a counterclockwise circulation and sea level setup similar to that described above, with strong sea level

gradient along the continental coast (Prandle 1975, Timmerman 1977, Mathisen & Johansen 1983, and Bijl 1997).

In this paper, we only consider the model response to monthly-mean wind stress. Since the response of the shallow North Sea to changing winds is the period of the first external mode sea level oscillation, on the order of several days, we may consider a mean monthly flow to be in a steady state. This approach is justified because we are investigating the sea level set up by wind forcing on seasonal and longer time scales, which vary much more slowly than the adjustment time of the North Sea to changes in winds. For each wind stress forcing that is used, the model is spun up from rest by increasing the wind stress forcing linearly from zero (ramping) over one inertial period (0.61 days) and then keeping it constant. When the spatially constant annual average wind stress forcing was used, the resulting model flow regime was almost in a steady state balance after one day, as evidenced by plots of currents and sea level at one, three, and five days. For this reason, it was decided that three days of simulation are enough to bring the model to a steady state with any monthly wind stress forcing.

Thus, a three-day simulation with steady wind stress forcing was made for each of the 480 individual months Jan. 1958 through Dec. 1997. The values of the model water levels at the grid points closest to selected coastal stations (see Fig. 1) were written out at the end of each three-day simulation to represent the value for that month.

## 4. SEA LEVEL COMPARISONS

### 4.1 Seasonal signals

We now compare our North Sea model output, or the computed sea levels with those actual observed at the 10 stations mentioned above. We first examine the seasonal signals at the annual and semi-annual periods. To estimate the amplitude and phase of the seasonal signals, we simultaneously least-squares fit sine and cosine functions with the annual and semi-annual periods to the 40-year time series. The resultant sine and cosine functions are then converted into the form (amplitude) \*  $\sin(\omega t + \text{phase})$ , where  $t=0$  refers to the nominal epoch of January 15.5.

Fig. 4 shows a comparison between the computed and observed annual and semi-annual

amplitude/phase as a function of latitude for the ten coastal stations. It is seen that:

(i) The observed annual amplitudes are between 5-15 mm, increasing almost monotonically towards the north and east. The corresponding computed amplitudes follow the same trend but are smaller by about a factor of 3.

(ii) The observed semi-annual amplitudes are between 1-3 mm, also increasing towards the north and east. The corresponding computed amplitudes follow the same trend but are smaller by a factor of about 2.

(iii) In general the computed seasonal phase agrees well with the observed for both annual and semi-annual signals, except for the annual phase of the southernmost stations.

Some of the main features above have been discussed previously by Tsimplis *et al.* (1994) and Xie & Dickman (1996). The difference in the seasonal amplitudes is expected because our computed values are only those caused by surface wind stress. There are other important factors that contribute significantly to the seasonal signals that are observed. The most important is presumably the steric effect due to thermal and salinity variations particularly in the surface water layers. The strength of air pressure effects on the sea level, such as in the form of the inverted-barometer effect, also varies seasonally. Furthermore, the annual and semi-annual ocean tides due to the sun's tidal force have centimeter level amplitudes. Another interesting possible contributor is actually the pole tide: Since the Earth's polar motion contains an annual wobble besides the 14-month Chandler wobble and nearly equal in amplitude, the annual wobble should presumably generate a pole tide of a half centimeter at maximum just like the Chandler wobble would.

It is interesting, then, that the seasonal phase estimates agree quite well, and that the computed and observed seasonal amplitudes show the same geographical trend. This presumably indicates that the sum of other seasonal effects are highly correlated with that of the wind-forcing contribution.

#### 4.2 Non-seasonal, broad-band signal

Next, we remove by subtraction the seasonal signals from all (monthly) time series, in order to concentrate on non-seasonal, broad-band signals. We also remove any linear trend in the time series, whatever the cause of the trend may be. The latter may include eustatic sea level rise, post-glacial or local movements of the ground, or even systematic observational errors. These are outside the interest of the present study.

Comparing such non-seasonal broad-band signals, we find the following:

(i) The computed sea level variation agrees remarkably well with the observed at the northern stations, while it becomes somewhat larger than the observed in overall amplitude for the southern stations. This is evident in Fig. 5 (and Table 1 below).

(ii) Table 1 lists the correlation coefficients between the computed and the observed time series. The geographical trend is obvious: the correlation is very high for the northern stations, while decreases rapidly toward the southernmost stations. The cross-correlation functions (not shown) all look characteristically similar to Fig. 7 below.

(iii) Since the cross-correlation only compares the “pattern” of the time series and conveys no information about the overall size of the amplitude, we should calculate the ratio [standard deviation of computed amplitude]/[standard deviation of observed amplitude]. The latter are also listed in Table 1. The ratio is close to one, except for the few southernmost stations.

Findings (ii) and (iii) confirm (i) in a quantitative manner. We conclude here that, while it tends to over-predicts the amplitude for the southernmost stations, our North Sea model using NCEP wind stress input predicts well the non-seasonal sea level variations along the Denmark-Netherlands coast. The latter is indeed where the strongest 14-month tide is found.

Thus, we now concentrate on the five northernmost stations. We simply average the five time series into a “composite” series, and make comparisons between the computed and the observed sea levels. Fig. 6 shows the two composite series; remarkable matching is already evident. Fig. 7 gives their (time-domain) cross-correlation as a function of time shift between the two series. A sharp peak at zero time-shift represents a correlation coefficient as high as 0.86. The correlation drops to near-zero with time shifts of only 1 month (the time resolution of our study) and longer. A spectral decomposition of this correlation is given in Fig. 8. It shows the (frequency-domain) coherence spectrum of the two composite series. The coherence spectrum is computed using the multi-taper spectral technique (Thomson 1982; also, e.g., Chao & Eanes 1995), which provides robust, minimum-leakage spectral estimates. Seven orthogonal tapers with time-bandwidth product of  $4\pi$  were adopted. The coherence across the entire spectrum is much higher than, say, the 99% confidence level (0.54 in the present case, see Chao & Eanes 1995). The phase difference remains no more than  $\pm 20^\circ$ .

For the same reason as in Finding (iii) above, we conduct a comparison of the individual spectra. Fig. 9 shows the two Fourier power spectra, again computed by means of the multi-taper technique.

Consistent with Tsimplis *et al.*'s (1994) model results, a very good match is evident across the entire spectral band to the Nyquist frequency, indicating the agreement of the power, or the size of the amplitude of the two (composite) time series.

Alternatively, one can show the time-varying spectral behavior of a time series by way of its time-frequency wavelet spectrum. The wavelet analysis was introduced to represent functions that are localized in time and frequency (Morlet *et al.* 1982). Using the Morlet wavelet, the result is shown in Fig. 10 (cf. Chao & Naito 1995). Here the contours indicate the strength of undulations at any particular frequency (or period) as a function of time going horizontally on the plot. High contrasts in shade indicate strong undulations; the brighter contour closures indicate positive amplitude and the darker ones the negative amplitude. We have to an extent saturated the grey scale in order to bring out the finer features.

Let's now examine Figs. 8-10 in more detail. In Fig. 8, a frequency band where the coherence dips below 99% (and the associated phase shows some "anomalous" behavior) is around the biennial period. This appears to be insignificant, however, as the signal power is rather low in this frequency band (in fact, the lowest among the entire frequency band, see Fig. 9a). It simply stems from low signal-to-noise ratio in this band and the resultant numerical instability. The same applies to the zero and near-zero frequencies, because the mean and a linear trend have been removed beforehand.

Figs. 9 and 10 reveal some interesting periodicities in the sea level records. There are prominent spectral peaks and strong undulations common to both the computed and observed sea levels at periods of around 7 years, 3 years (especially during the first half of the records), 14 months, 9 months, and 6.5 months. They all correspond to the peaks detected in the original eastward wind in Fig. 2, except the 7-year quasi-periodicity. As stated earlier, these features presumably are part of the regional climatology associated with the North Atlantic Oscillation system. Note that the 6.5 month is close to half the 14-month periodicity and the 7-month quasi-periodicity reported by Naito & Kikuchi (1992) in global atmospheric angular momentum.

The 7-year quasi-periodicity is relatively weak in our computed output, and certainly much weaker than the observed (see Fig. 9). The corresponding band, in fact, is the only frequency band where exists a major discrepancy in the spectral comparison of Fig. 9. The interesting feature, however, is that their relative behavior around this period seems highly correlated as revealed by the high coherence (Fig. 9) and similar wavelet spectra (Fig. 10). Thus, the causes for the discrepancy may be the excessive low-frequency smoothing of the NCEP stress field, or the existence of other

unmodeled forcing mechanism which is highly correlated with the wind-forcing such as air-sea temperature differences. In any event, this is outside of our present interest. A relatively smaller discrepancy in Fig. 9 exists around the 9-month peak. The above causes may play a role, but note that the relative size of the difference in amplitude is only on the order of 30%. At all other frequencies the computed sea level matches the observed quite well. This is to be further discuss below.

## 5. CONCLUSIONS

We have used the 40-year (1958-1997), monthly surface stress field in the North Sea region derived by NCEP as input to a barotropic North Sea model with realistic geography, bathymetry, and boundary conditions. The output wind-driven sea level variations are compared with 10 tide gauge records along the continental coast. Besides the strong seasonal variations, several prominent quasi-periodicities exist at around 7 years, 3 years, 14 months, 9 months, and 6.5 months.

Correlation and spectral analyses show remarkable agreement between the model output and the observations, across almost the entire frequency band (out to the Nyquist frequency), except at the seasonal periods and periods longer than about 7 years. Our study only pertains to wind-driven sea level variations. The seasonal discrepancy presumably originates from other meteorological causes than wind-forcing that exist in the observation but are not modeled in our study. The long-period discrepancy may also have meteorological causes.

Our focus here is the 14-month tide, which has been observed to be as large as 3 cm in amplitude along the Denmark-Netherlands coast. In the past both wind-forcing and certain North-Sea resonance-enhancement of the Chandler pole tide have been examined to explain this tide. Our present findings strongly supports the wind-forcing mechanism as the major cause of the 14-month tide. To be sure, a 14-month pole tide (and an annual pole tide for that matter) should in general be present; it's equilibrium amplitude is no more than 0.5 cm. It was stated earlier that the computed sea level amplitude depends on the model parameterization and the wind stress forcing. The fact that in our simulation the amplitude matches across the entire frequency band indicates that the parameterization adopted here is realistic, and having no preference or "favor" towards the matching at the 14-month periodicity of interest here. In other words, we find no evidence to support an anomalous behavior of the North Sea in this particular band, and hence no need to invoke a geophysical explanation involving resonance-enhancement of pole tide to explain the observations.

## **ACKNOWLEDGMENTS**

We thank NCEP for providing the 40-year wind field data over the Internet, and Hua-Lu Pan for information about the NCEP model surface layer parameterization. This work was partially supported by the NASA Solid Earth and Natural Hazards Program. One of the authors (WPO) was funded through a University Corporation for Atmospheric Research (UCAR) Visiting Scientist appointment.

## REFERENCES

- Backhaus, J.O. & Maier-Reimer, E., 1983. On seasonal circulation patterns in the North Sea, in *North Sea Dynamics, Proceedings of the Intl. Symposium on North Sea Dynamics, Hamburg, Aug. 31-Sept. 4, 1981*, pp. 63-84, eds Sundermann, J. & Lenz, W., Springer-Verlag, New York, NY.
- Bijl, W., 1997. Impact of a wind climate change on the surge in the southern North Sea, *Climate Res.*, **8**, 45-59.
- Blumberg, A.F. & Mellor, G.L., 1987. A description of a three-dimensional coastal ocean circulation model, in *Three-Dimensional Coastal Ocean Models, Coastal and Estuarine Sciences 4*, pp. 1-16, ed Heaps, N.S., American Geophysical Union, Washington, DC.
- Bryson, R.A. & Starr, T.B., 1977. Chandler tides in the atmosphere, *J. Atmos. Sci.*, **34**, 1975-1986.
- Carton, J.A. & Wahr, J.M., 1986. Modelling the pole tide and its effect on the Earth's rotation, *Geophys. J. R. astr. Soc.*, **84**, 121-137.
- Chao, B. F. & Eanes, R. J., 1995. Global gravitational change due to atmospheric mass redistribution as observed in Lageos' nodal residual, *Geophys. J. Int.* **122**, 755-764.
- Chao, B. F. & Naito, I., 1995. Wavelet analysis provides a new tool for studying Earth's rotation, *EOS, Trans. Amer. Geophys. Union*, **76**, 161-165.
- Davies, A.M., 1982. Meteorologically-induced circulation on the North-West European continental shelf: from a three-dimensional numerical model, *Oceanol. Acta*, **5**, 269-280.
- Dickman, S.R., 1985. The self-consistent dynamic pole tide in global oceans, *Geophys. J. R. astr. Soc.*, **81**, 157-174.
- Dickman, S.R., 1988. The self-consistent dynamic pole tide in non-global oceans, *Geophys. J. R. astr. Soc.*, **94**, 519-543.
- Dickman, S.R. & Preisig, J.R., 1986. Another look at North Sea pole tide dynamics, *Geophys. J. R. astr. Soc.*, **87**, 295-304.
- Ekman, M. & Stigebrandt, A., 1990. Secular change of the seasonal variation in sea level and of the pole tide in the Baltic Sea, *J. Geophys. Res.*, **95**(C4), 5379-5383.
- Flather, R.A., 1984. A numerical model investigation of the storm surge of 31 January and 1 February 1953 in the North Sea, *Quart. J. R. Meteor. Soc.*, **110**, 591-612.
- Flather, R., Proctor, R. & Wolf, J., 1991. Oceanographic forecast models, in *Computer Modeling in the Environmental Sciences*, pp. 15-30, eds Farmer, D.G., & Rycroft, M.J., Clarendon Press.
- Furnes, G.K., 1980. Wind effects in the North Sea, *J. Phys. Oceanogr.*, **10**, 978-984.

- Haltiner, G.J. & Williams, R.T., 1980. *Numerical Prediction and Dynamic Meteorology, 2d ed.*, John Wiley & Sons, Inc., New York, 477 pp.
- Hellerman, S., 1967. An updated estimate of the wind stress on the world ocean, *Mon. Wea. Rev.*, **95**, 607-626. Correction, *Mon. Wea. Rev.*, **96**, 62-74.
- Kalnay, E., Kanamitsu, M., Kistler, R., Collins, W., Deaven, D., Gandin, L., Iredell, M., Saha, S., White, G., Woollen, J., Zhu, Y., Chelliah, M., Ebisuzaki, W., Higgins, W., Janowiak, J., Mo, K.C., Ropelewski, C., Wang, J., Leetmaa, A., Reynolds, R., Jenne, R. & Joseph, D., 1996. The NCEP/NCAR 40-year reanalysis project, *Bull. Amer. Meteor. Soc.*, **77**(3), 437-471.
- Korevaar, C.G., 1990. *North Sea Climate Based on Observations from Ships and Lightvessels*, Kluwer Academic Publishers, Dordrecht, 137 pp.
- Lambeck, K., 1980. *The Earth's Variable Rotation, Geophysical Causes and Consequences*, Cambridge University Press, 449 pp.
- Maier-Reimer, E. 1977. Residual circulation in the North Sea due to the M2 tide and mean annual wind stress, *Deut. Hydrog. Zeit.*, **30**, 69-80.
- Marple, L., 1990. A new autoregressive spectrum analysis algorithm, *IEEE Trans. Acoust. Speech Signal Process.*, **28**, 441-454.
- Mathisen, J.P. & Johansen, O., 1983. A numerical tidal and storm surge model of the North Sea, *Marine Geodesy*, **6**, 267-291.
- Mestas-Nunez, A.M., Chelton, D.B., Freilich, M.H. & Richman, J.G., 1994. An evaluation of ECMWF-based climatological wind stress fields, *J. Phys. Oceanogr.*, **24**, 1532-1549.
- Miller, S.P., 1973. Observations and interpretation of the pole tide, MSc thesis, Massachusetts Institute of Technology, 97 pp.
- Miller, S.P. & Wunsch, C., 1973. The pole tide, *Nature Physical Science*, **246**, 98-102.
- Morlet, J., Arehs, G, Fourgeau, I., & Giard, D., 1982. Wave propagation and sampling theory, *Geophysics*, **47**, 203-236.
- Naito, I., & Kikuchi, N., 1992. Atmospheric contributions to non-seasonal variations in the length of day, *Geophys. Res. Lett.*, **19**, 1843-1846.
- O'Connor, W.P., 1986. The 14-month wind stressed residual circulation (pole tide) in the North Sea, *NASA TM-87800*, 23 pp.
- Pattullo, J., Munk, W., Revelle, R. & Strong, E., 1955. The seasonal oscillation in sea level, *J. Mar. Res.*, **14**, 88-155.

- Pingree, R.D. & Griffiths, D.K., 1980. Currents driven by a steady uniform wind stress on the shelf seas around the British Isles, *Oceanol. Acta.*, **3**, 227-236.
- Prandle, D., 1975. Storm surges in the southern North Sea and River Thames, *Proc. R. Soc. Lond.*, **A344**, 509-539.
- Prandle, D., 1978. Residual flows and elevations in the southern North Sea, *Proc. R. Soc. Lond.*, **A359**, 189-228.
- Prandle, D., 1984. A modeling study of the mixing of  $^{137}\text{Cs}$  in the seas of the European continental shelf, *Phil. Trans. R. Soc. Lond.*, **A310**, 407-436.
- Rossiter, J.R., 1967. An analysis of annual sea level variations in European waters, *Geophys. J. R. astr. Soc.*, **12**, 259-299.
- Stammer, D., Tokmakian, R., Semtner, A. & Wunsch, C. 1996. How well does a 1/4 degree global circulation model simulate large-scale oceanic observations? *J. geophys. Res.*, **101**, 25779-25811.
- Smith, S.D., Anderson, R.J., Oost, W.A., Kraan, C., Maat, N., DeCosmo, J., Katsaros, K.B., Davidson, K.L, Bumke, K., Hasse, L. & Chadwick, H.M., 1992. Sea surface wind stress and drag coefficients: the HEXOS results, *Bound.-Layer Meteor.*, **60**, 109-142.
- Sundermann, J. & Lenz, W., eds, 1983. *North Sea Dynamics, Proceedings of the Intl. Symposium on North Sea Dynamics, Hamburg, Aug. 31-Sept. 4, 1981*, Springer-Verlag, New York, NY, 693 pp.
- Thomson D. J., 1982. Spectrum estimation and harmonic analysis, *Proc. IEEE*, **70**, 1055-1096.
- Timmerman, H., 1977. *Meteorological Effects on Tidal Heights in the North Sea, Mededelingen en Verhandelingen, No. 99*, Koninklijk Nederlands Meteorologisch Instituut, 105 pp.
- Trenberth, K.E., Large, W.G. & Olson, J.G., 1989. The effective drag coefficient for evaluating wind stress over the oceans, *J. Climate*, **2**, 1507-1516.
- Trupin, A. & Wahr, J., 1990. Spectroscopic analysis of global tide gauge sea level data, *Geophys. J. Int.*, **100**, 441-453.
- Tsimplis, M.N., Flather, R.A. & Vassie, J.M., 1994. The North Sea pole tide described through a tide-surge numerical model, *Geophys. Res. Lett.*, **21**, 449-452.
- Verboom, G.K., de Ronde, J.G. & van Dijk, R.P., 1992. A fine grid tidal flow and storm surge model of the North Sea, *Cont. Shelf Res.*, **12**, 213-233.
- Wallace J. M., and Gutzler D. S. (1981) Teleconnections in the geopotential height field during the northern hemisphere winter, *Mon. Wea. Rev.*, **109**, 784-812.

WASA Group, 1998. Changing Waves and Storms in the Northeast Atlantic? *Bull. Am. Meteor. Soc.*, **79**, 741-760.

Wunsch, C., 1974. Dynamics of the pole tide and the damping of the Chandler wobble, *Geophys. J. R. astr. Soc.*, **39**, 539-550, Correction (1975), *Geophys. J. R. astr. Soc.*, **40**, 311.

Wunsch, C., 1986. Dynamics of the North Sea pole tide reconsidered, *Geophys. J. R. astr. Soc.*, **87**, 869-884.

Wunsch, C., Haidvogel, D.B., Iskandarani, M. & Hughes, R., 1997. Dynamics of the long-period tides, *Prog. Oceanog.*, **40**, 81-108.

Xie, L. & Dickman, S.R., 1995. North Sea pole tide dynamics, *Geophys. J. Int.*, **121**, 117-135.

Xie, L. & Dickman, S.R., 1996. Tide gauge data analysis of the pole tide in the North Sea, *Geophys. J. Int.*, **126**, 863-870.

Table 1. The ten North Sea tide gauge stations used in this study. The last two columns respectively list the correlation coefficients between the computed and the observed non-seasonal sea level signals, and the ratio [standard deviation of computed amplitude]/[standard deviation of observed amplitude].

Station	Latitude	Longitude	Corr. Coef.	STD ratio
Esbjerg, Denmark	55°N 28'	8°E 26'	0.880	0.90
West-Terschelling, Netherlands	53°N 22'	5°E 13'	0.784	1.07
Delfzijl, Netherlands	53°N 20'	6°E 56'	0.885	0.95
Harlingen, Netherlands	53°N 10'	5°E 25'	0.833	0.93
Den Helder, Netherlands	52°N 58'	4°E 45'	0.759	1.11
Ijmuiden, Netherlands	52°N 28'	4°E 35'	0.735	1.26
Hoek Van Holland, Netherlands	51°N 59'	4°E 7'	0.730	1.35
Maassluis, Netherlands	51°N 55'	4°E 15'	0.712	1.24
Vlissingen, Netherlands	51°N 27'	3°E 36'	0.674	1.70
Oostende, Belgium	51°N 14'	2°E 55'	0.462	1.76

## Figure Captions:

Figure 1. (a) Map of Europe showing the North Sea region modeled in this study. (b) The modeled North Sea region with depth contours in meters. The crosses indicate locations of the ten Permanent Service for Mean Sea Level tide gauge stations on the continental coast examined in this study (see Table 1), including the northern five Denmark-Netherlands coastal stations (marked by  $\otimes$ ), where the 14-month tide is the strongest (and used to form the composite record later). Overlain as thick arrows are the 40-year (1958-1997) averaged wind stress field at NCEP grid points.

Figure 2. (a) The 40-year time series of the horizontal wind velocity in the North Sea region, spatially averaged over the NCEP grid points;  $u$ : eastward component;  $v$ : northward component (shifted by -20 m/s in the plot). (b) Their maximum-entropy power spectra.

Fig. 3. Sea level contours in centimeter, and currents driven by the 40-year average NCEP wind stress (Fig. 1), predicted by our North Sea ocean model.

Figure 4. (a) Comparison of the annual signal of computed (\*) wind-driven sea level with that observed (O), in terms of amplitude and phase as a function of the latitude of the ten coastal stations. (b) Same as (a) but for the semi-annual signals.

Figure 5. Comparison of computed (top curves, vertically shifted) wind-driven sea level with that observed (bottom curves) after the removal of seasonal (annual and semi-annual) signals and a linear trend, shown for four randomly selected stations.

Figure 6. Comparison of the computed (top curve, vertically shifted) and observed (bottom curve) “composite” average sea level of the five Denmark-Netherlands coastal stations, after the removal of seasonal (annual and semi-annual) signals and a linear trend.

Figure 7. The (time-domain) cross-correlation function between the two series in Fig. 6.

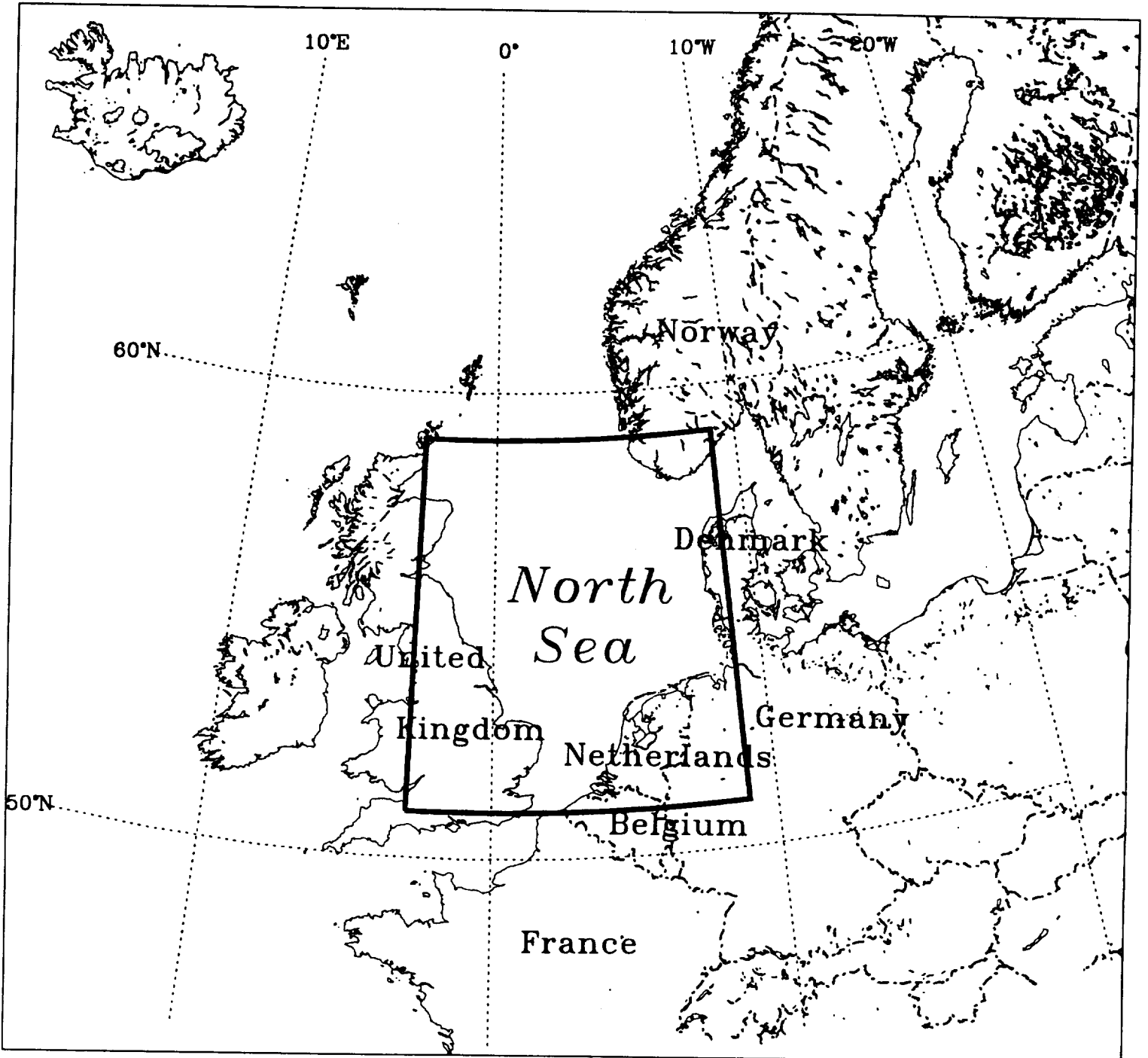
Figure 8. The (frequency-domain) coherence spectrum between the two series in Fig. 6. Upper panel: coherence amplitude squared compared with the 99% confidence level; Lower panel: coherence phase.

Figure 9. The (multi-tapered) power spectra for the two series in Fig. 6.

Fig. 10. The (time-frequency) wavelet spectra for the two series in Fig. 6 (upper panel: computed; lower panel: observed). The contours indicate the strength of undulations at any particular frequency (or period) as a function of time. The brighter contour closures indicate positive amplitude and the darker ones the negative amplitude.

Fig. 1(a)

(a)



(b)

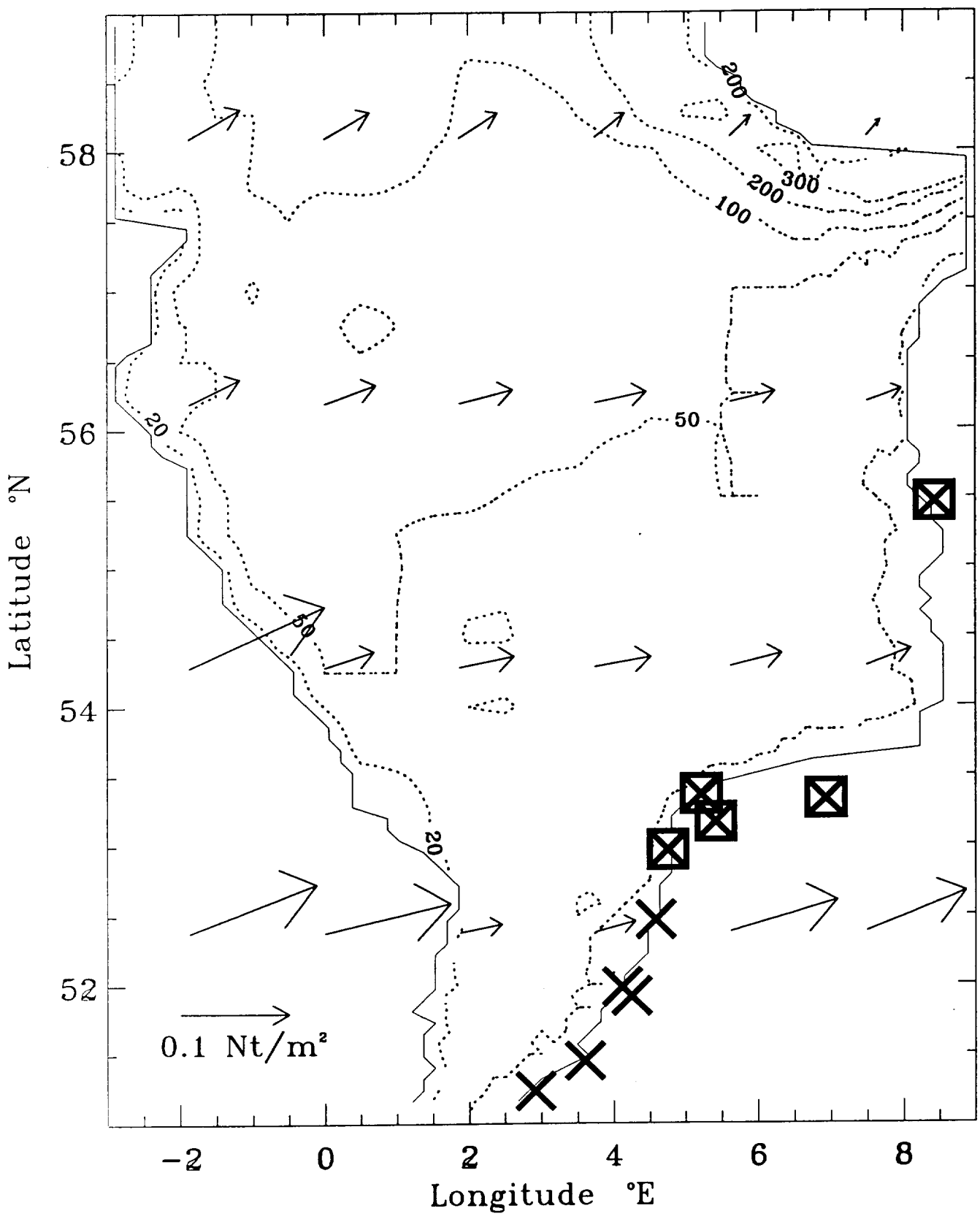


Fig 2(a)

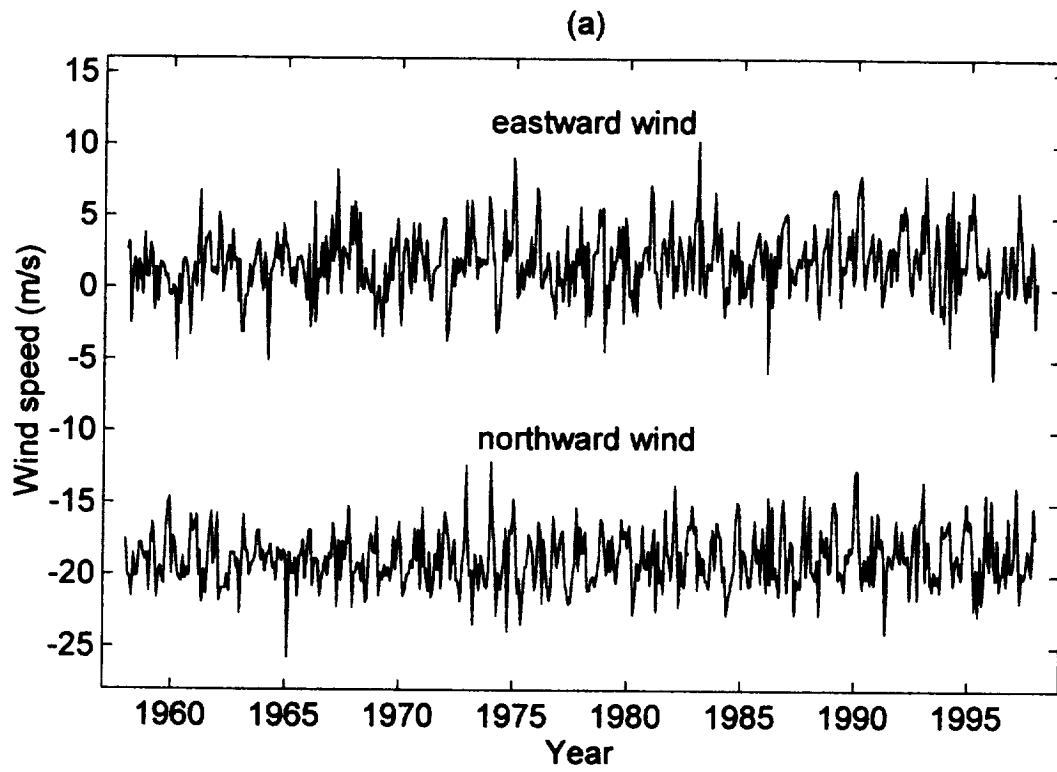


Fig 2 (b)

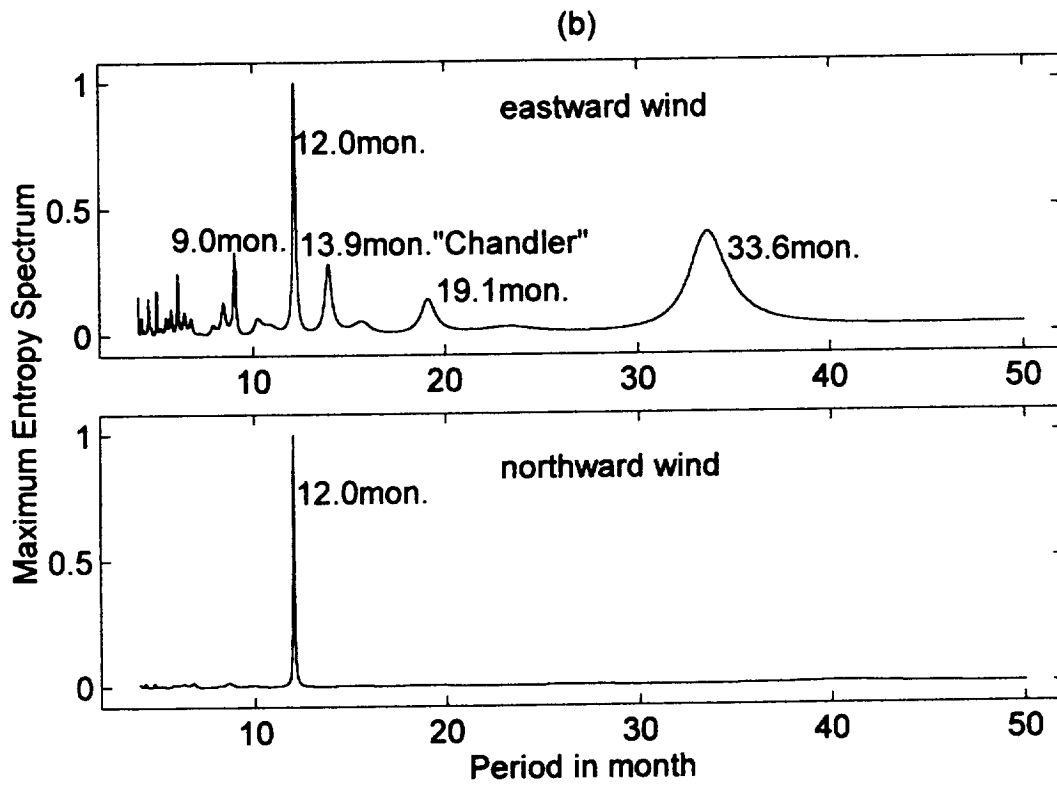


Fig 3

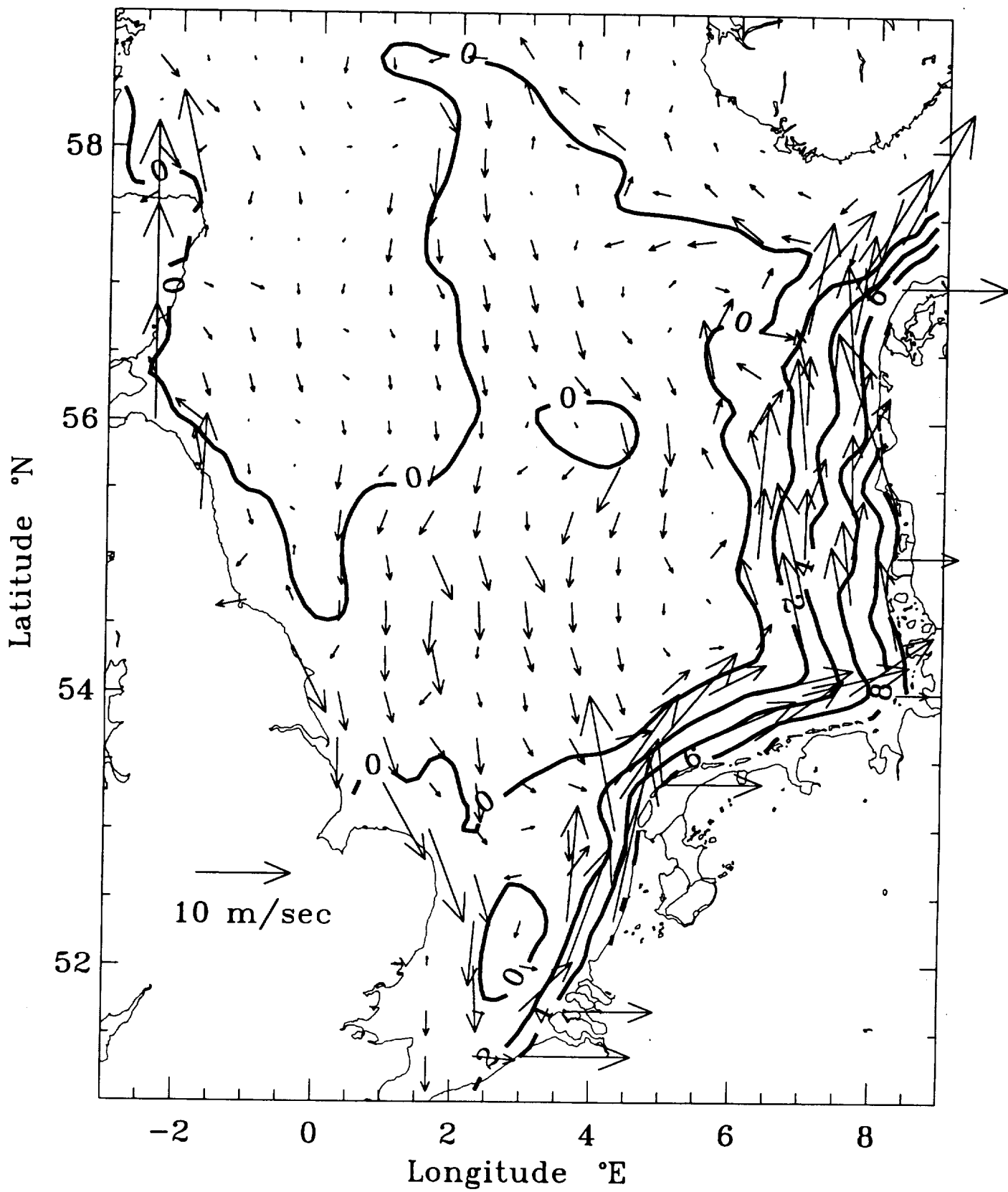


Fig. 4(a)

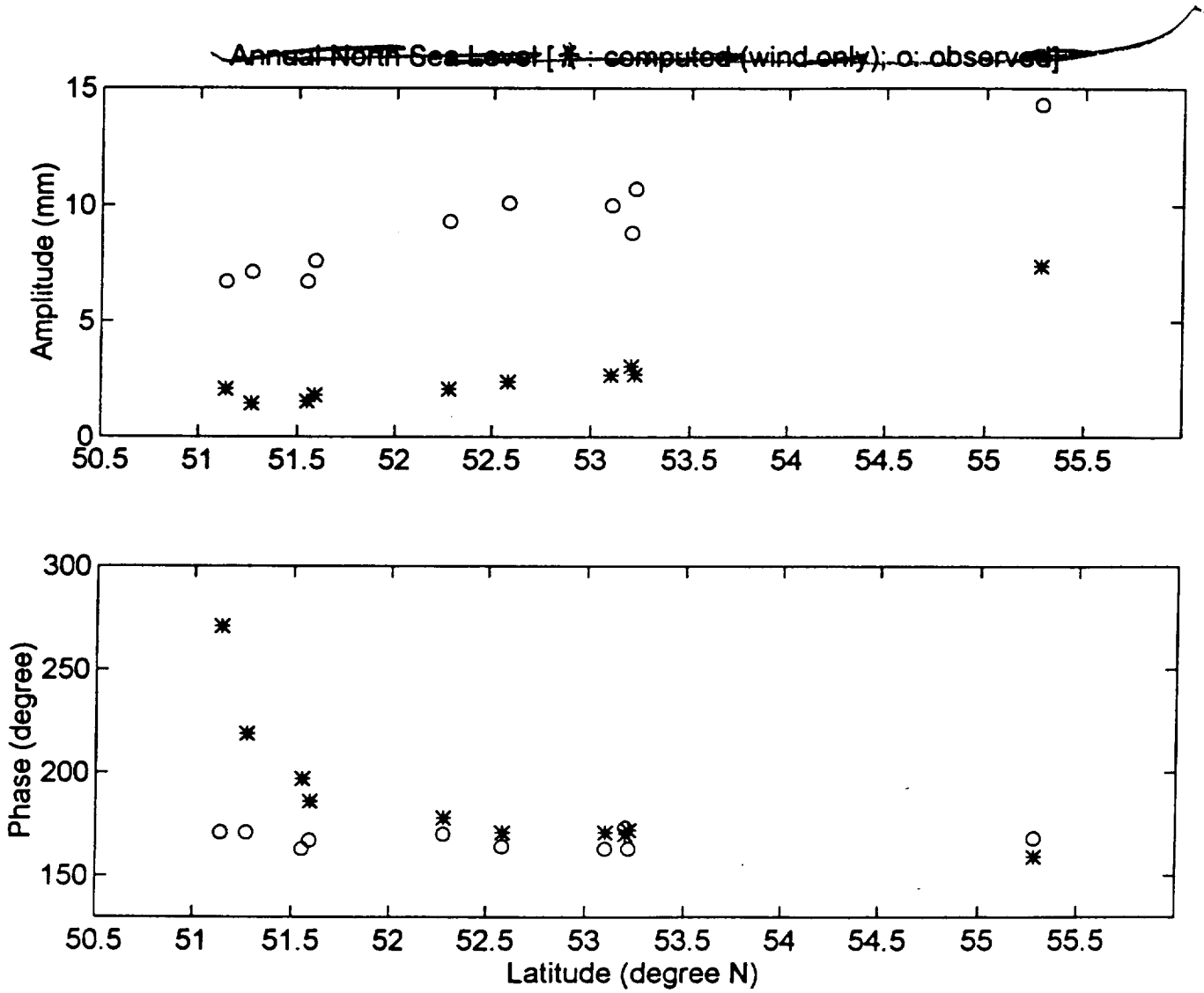


Fig. 4 (b)

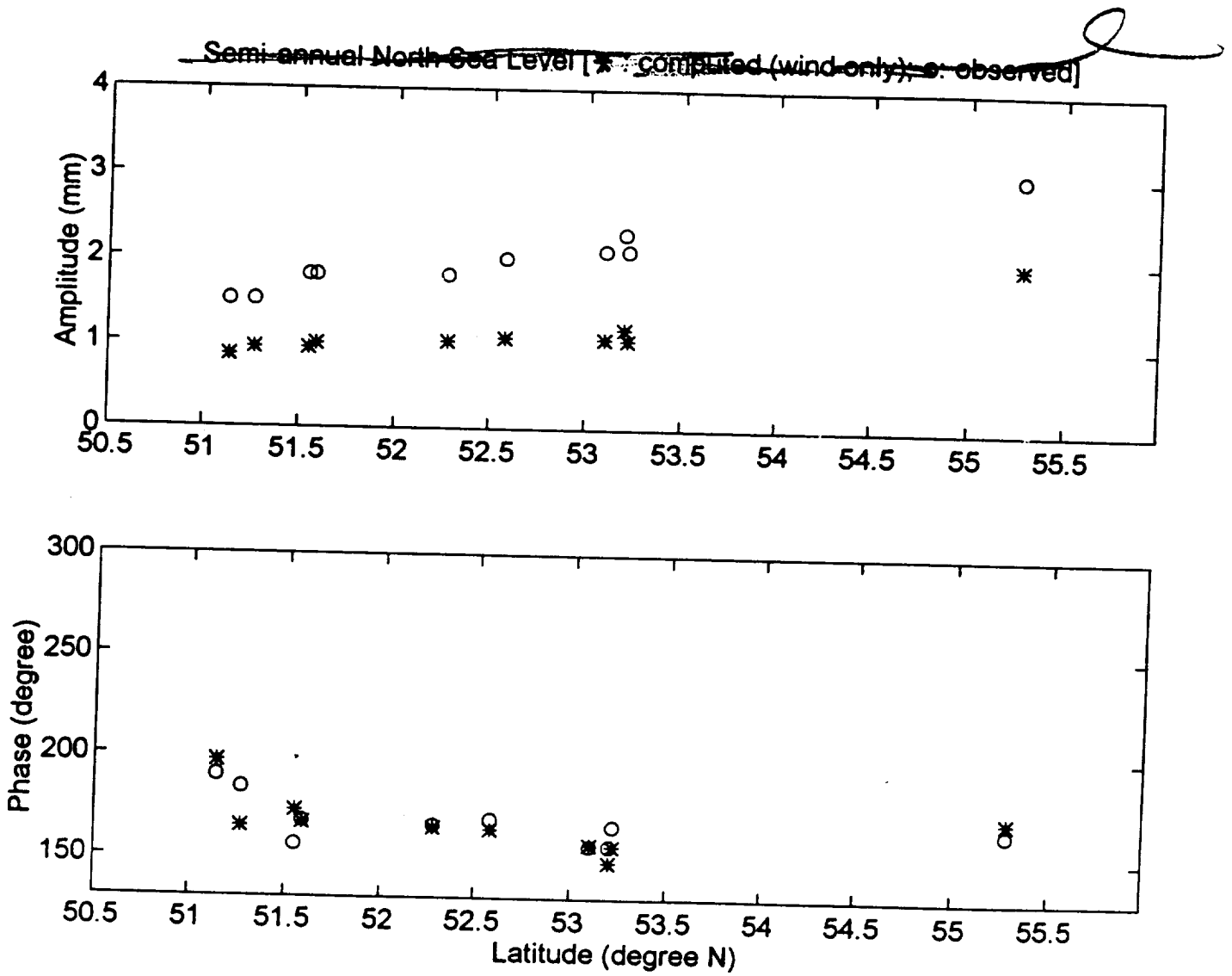


Fig. 5

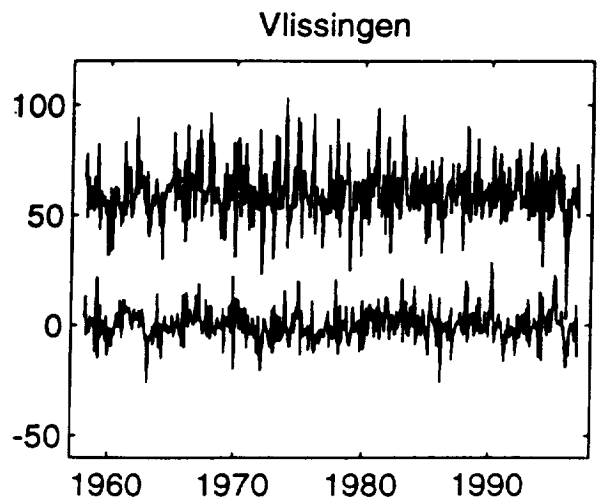
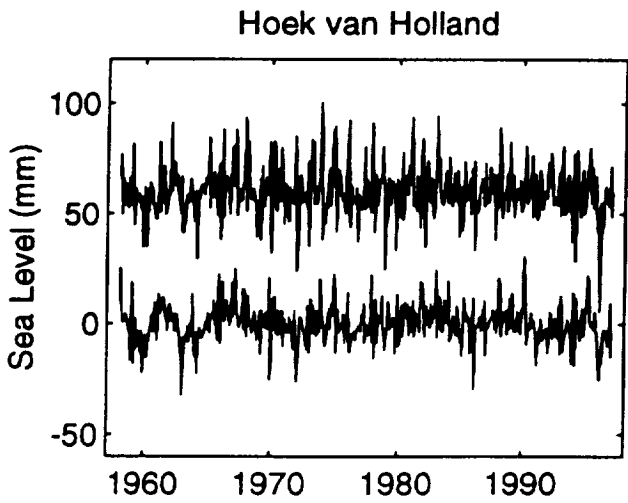
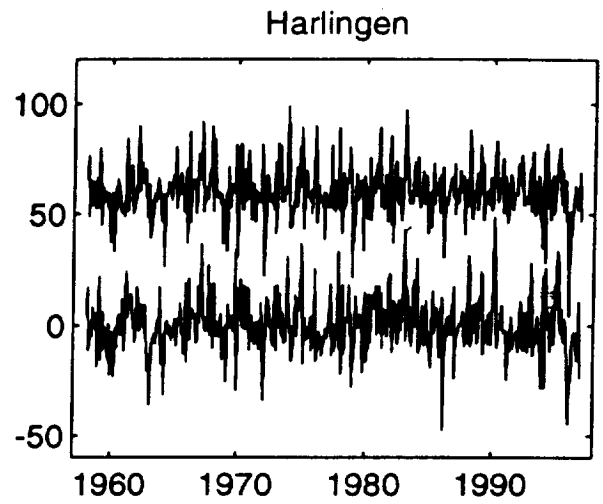
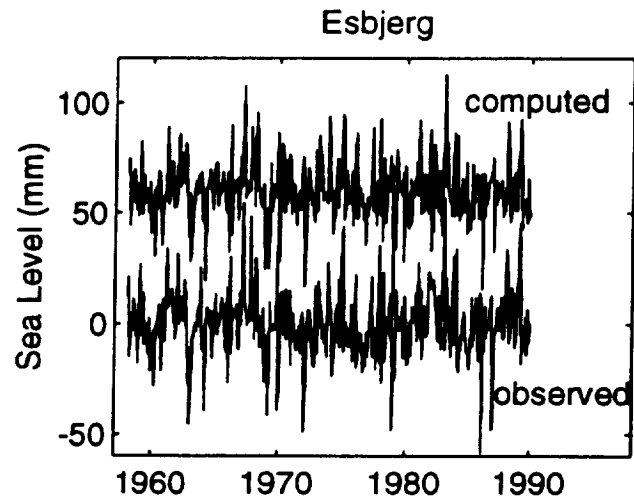


Fig. 6

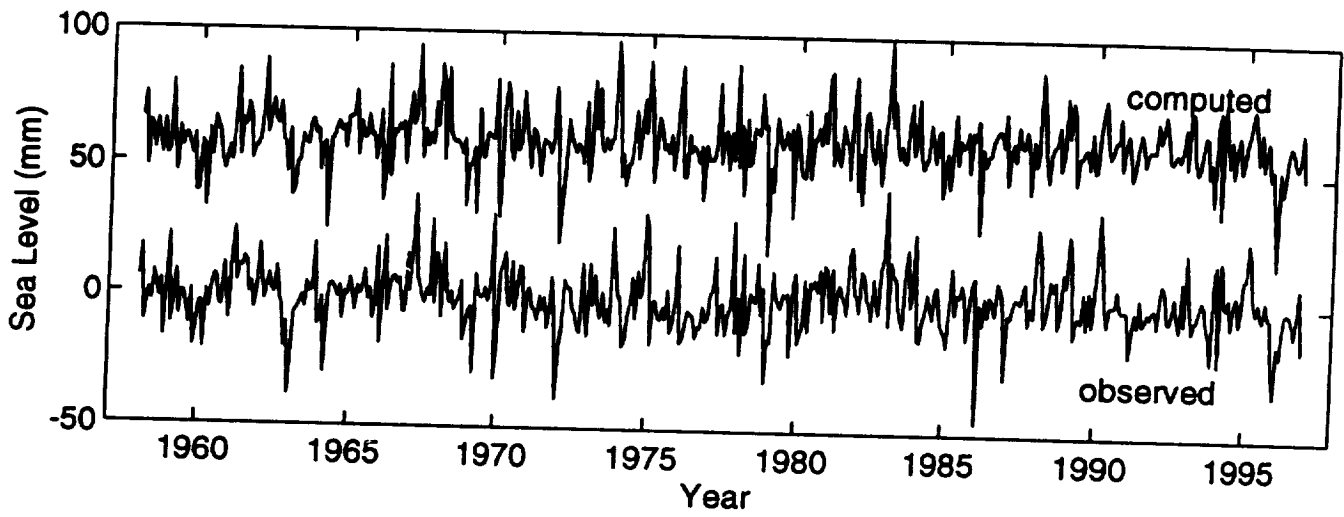


Fig. 7

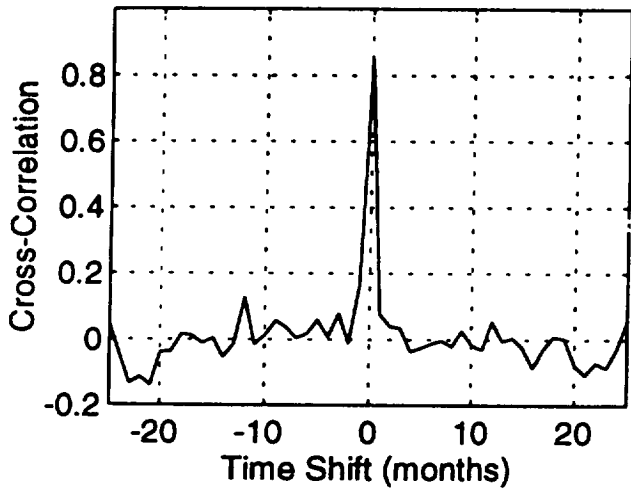


Fig. 8

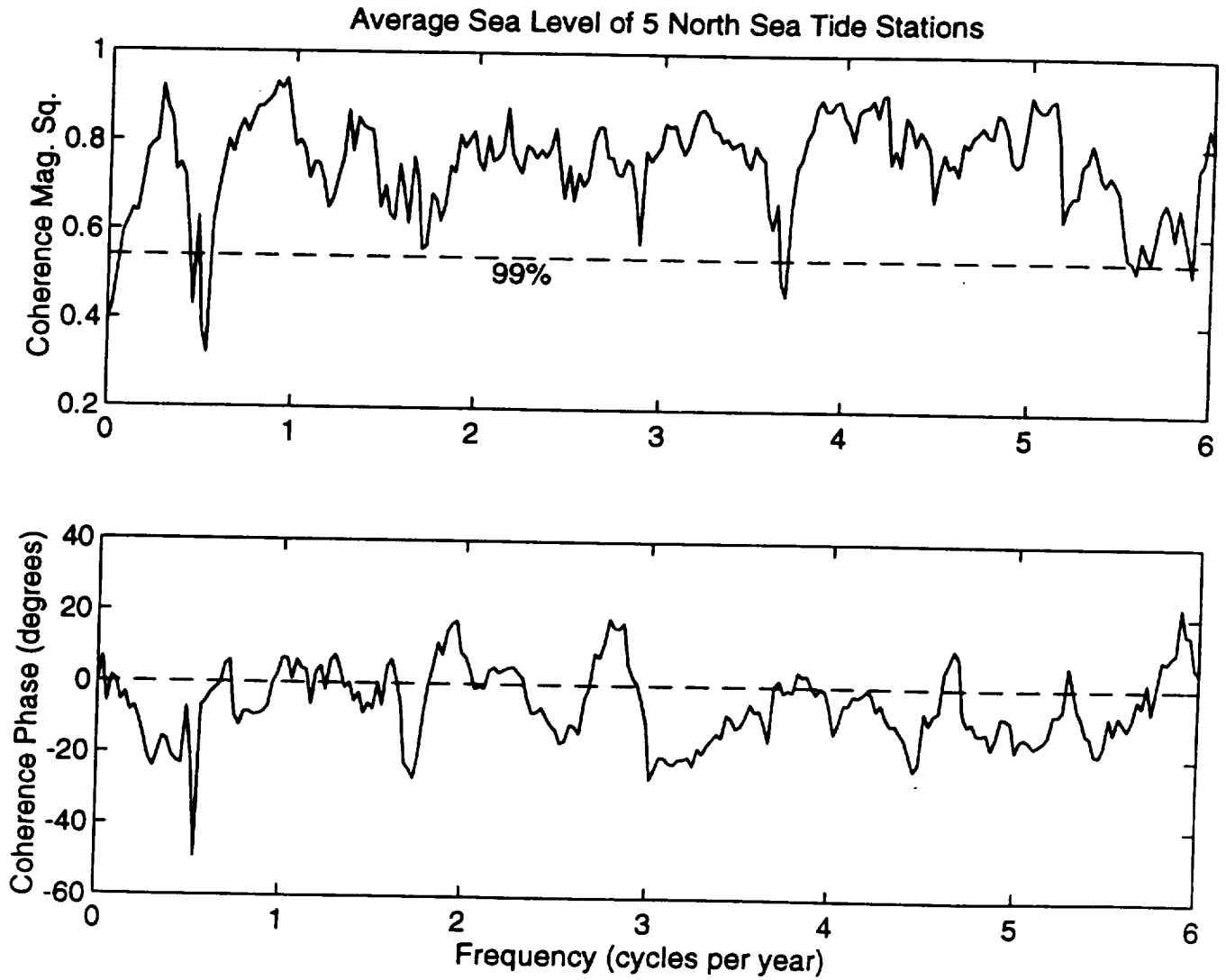


Fig. 9

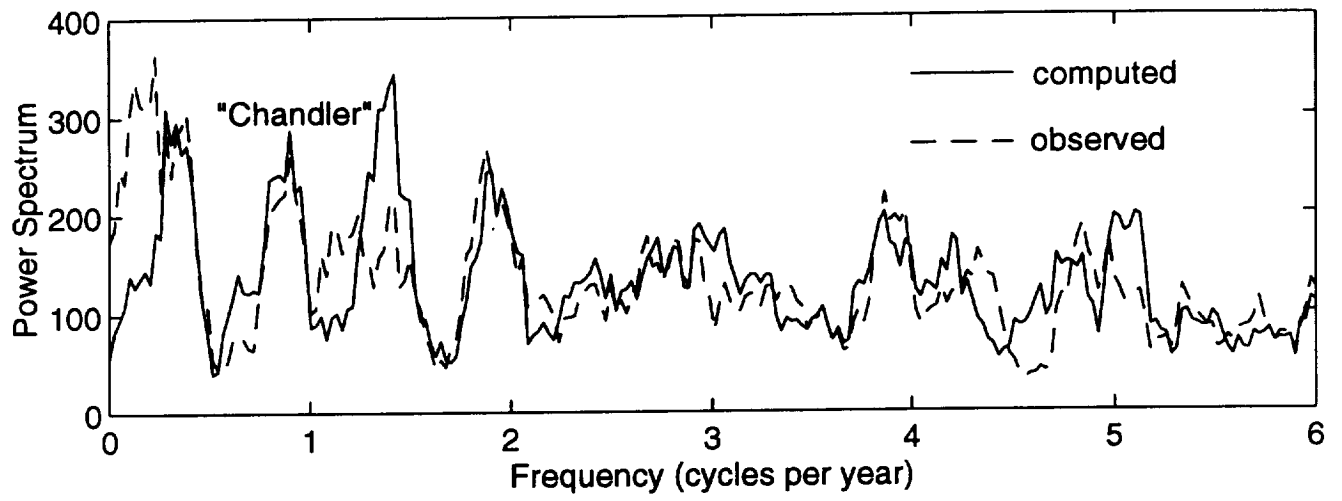


Fig 10  
c

